Synthesis, Electronic Structure, and Novel Reactivity of Strained, Boron-Bridged [1]Ferrocenophanes

Andrea Berenbaum,[‡] Holger Braunschweig,*[,§] Regina Dirk,[§] Ulli Englert,[§] Jennifer C. Green,*[,†] Frieder Jäkle,[‡] Alan J. Lough,[‡] and Ian Manners*[,‡]

Contribution from the Department of Chemistry, University of Toronto, 80 St. George Street, Toronto M5S 3H6, Ontario, Canada, Institut für Anorganische Chemie, Technische Hochschule Aachen, Templergraben 55, D-52056 Aachen, Germany, and Inorganic Chemistry Laboratory, University of Oxford, South Parks Road, Oxford OX1 3QR, U.K.

Received January 28, 2000

Abstract: The first boron-bridged [1]ferrocenophanes, Fe(η-C_5H_4)$_2$BN($SiMe_3$)$_2$ (**4a**), Fe(η-C_5H_4)$_2$BN(*t*Bu)-$SiMe_3$ (**4b**), and Fe(η-C_5H_4)$_2$BN*i*Pr_2 (**4c**), have been synthesized via reaction of Fe(η-C_5H_4Li)$_2$·*n*TMEDA (TMEDA = *N*,*N*,*N*′,*N*′-tetramethylethylenediamine) with the aminodichloroboranes $Cl_2BN(SiMe_3)_2$, Cl_2BN-(*t*Bu)$SiMe_3$, and Cl_2BN*i*Pr_2, respectively. Species **4a**, **4b**, and **4c** represent the first [1]ferrocenophanes containing a bridging first row element and were isolated in 35−44% yield as dark red crystalline solids which were characterized by multinuclear NMR and UV−vis spectroscopy, mass spectrometry, and single-crystal X-ray diffraction (**4a**,**c**). The tilt-angle between the planes of the cyclopentadienyl rings in **4a** and **4c** was found to be 32.4(2)° and 31.2(2)° (average), respectively. The angle of 32.4(2)° in **4a** represents the largest tilt reported to date for any [*n*]ferrocenophane. The ring-tilting results in a considerable redshift of the lowest energy absorbances in the UV−vis spectra recorded in hexanes (λ_{max} 479 (**4a**), 489 (**4b**), 498 nm (**4c**)) in comparison to ferrocene (λ_{max} = 440 nm). However, interestingly, the transitions are not as low energy as that for Fe(η-C_5H_4)$_2$S (**3**; λ_{max} = 504 nm), which shows a slightly smaller tilt angle of 31.1(1)°. As the nature of the bridging element appeared to influence the HOMO-LUMO gap, a comparative investigation of the electronic structures of **4a** and **3** was performed using Density Functional Theory (DFT). These calculations revealed that the HOMO-LUMO gap is indeed slightly larger in **4a** than in **3** as a consequence of mixing of the Fe−Cp antibonding orbitals with the B−C orbitals in **4** and the Fe d orbitals with the sulfur lone pair in **3**. The boron-bridged [1]ferrocenophanes **4b** and **4c** were found to readily undergo unprecedented ring-opening and insertion reactions with transition metal carbonyls at room temperature. Thus, reaction of **4c** with $Fe(CO)_4$-(THF) or $Fe_2(CO)_9$ led to insertion of an $Fe(CO)_4$ fragment into the Fe−Cp bond rather than the B−C bond yielding $(CO)_2$(μ-$CO)_2Fe_2$(η-C_5H_4)$_2$BN*i*Pr_2 (**7**), a novel boron-bridged analogue of *cis*-[CpFe$(CO)_2]_2$. Reaction of the analogous compound **4b** with $Co_2(CO)_8$ led to the formation of compound **8**, which consists of a CpCo-$(CO)_2$ fragment, and a Cp$(CO)_2$Fe−Co$(CO)_4$ fragment linked by a boron bridge. Compounds **4a**, **4b**, and **4c** undergo thermal ring-opening polymerization (ROP) at 180−200 °C to give the insoluble poly(ferrocenylborane)s [Fe(η-C_5H_4)$_2$BN($SiMe_3$)$_2$]$_n$ (**9a**) and [Fe(η-C_5H_4)$_2$BN(*t*Bu)$SiMe_3$]$_n$ (**9b**) and the soluble, low molecular weight polymer [Fe(η-C_5H_4)$_2$BN*i*Pr_2]$_n$ (**9c**) together with small quantities of cyclic dimers and trimers. The ROP enthalpy for **4a** was estimated to be ca. 95 kJ mol^{-1} by DSC measurements. This value is lower than expected, which we attribute to the presence of bulky substituents at boron.

Introduction

Highly strained organic molecules have been the focus of considerable attention from theoretical and structural perspectives and also from the standpoint of their reactivity which can, for example, lead to applications as polymer precursors.[1,2] In contrast, relatively few detailed studies have been performed on strained organometallic molecules, particularly those that contain transition elements. [1]Ferrocenophanes **1** represent unusual examples of strained species of this type in which the introduction of a single bridging element between the cyclopentadienyl ligands of ferrocene leads to a strained, ring-tilted structure.[3] These molecules have recently been the focus of attention as a result of their facile ring-opening reactions,[4] including ring-opening polymerization (ROP) to afford poly(ferrocenes) **2**.[5] The synthesis and study of strained ferro-

[‡] University of Toronto.
[§] Technische Hochschule Aachen.
[†] University of Oxford.

(1) (a) Wiberg, K. B. *Angew. Chem., Int. Ed. Engl.* **1986**, *25*, 312. (b) Bodwell, G. J. *Angew. Chem., Int. Ed. Engl.* **1996**, *35*, 2085.

(2) Greenberg, A.; Liebman, J. F. *Strained Organic Molecules*; Academic Press: New York, 1978.

(3) (a) Herberhold, M. *Angew. Chem., Int. Ed. Engl.* **1995**, *34*, 1837. (b) Manners, I. *Adv. Organomet. Chem.* **1995**, *37*, 131.

(4) (a) Fischer, A. B.; Kinney, J. B.; Staley, R. H.; Wrighton, M. S. *J. Am. Chem. Soc.* **1979**, *101*, 6501. (b) MacLachlan, M. J.; Bourke, S. C.; Lough, A. J.; Manners, I. *J. Am. Chem. Soc.* **2000**, *122*, 2126. (c) O'Brien, S.; Keates, J. M.; Barlow, S.; Drewitt, M. J.; Payne, B. R.; O'Hare, D. *Chem. Mater.* **1998**, *10*, 4088.

(5) (a) Foucher, D. A.; Tang, B.-Z.; Manners, I. *J. Am. Chem. Soc.* **1992**, *114*, 6246. (b) Manners, I. *Can. J. Chem.* **1998**, *76*, 371. (c) Manners, I. *Chem. Commun.* **1999**, 857. (d) Massey, J. A.; Power, K. N.; Winnik, M. A.; Manners, I. *Adv. Mater*. **1998**, *10*, 1559.

(6) Osborne, A. G.; Whiteley, R. H. *J. Organomet. Chem.* **1975**, *101*, C27.

(7) Rulkens, R.; Lough, A. J.; Manners, I. *Angew. Chem., Int. Ed. Engl.* **1996**, *35*, 1805.

10.1021/ja000311+ CCC: $19.00
Published on Web 06/21/2000

cenophanes and related species therefore represents a valuable opportunity to gain insight into this virtually unexplored area.

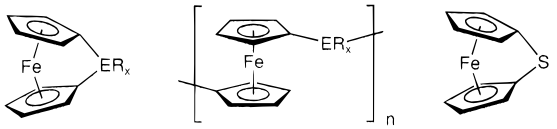

1 **2** **3**

The first [1]ferrocenophane (**1**, $ER_x = SiPh_2$), was synthesized and characterized in 1975 by Osborne and co-workers.[6] Subsequently, the range of [1]ferrocenophanes has been extended to those bridged with heavier main group elements of the second period and below such as group 14 (Ge, Sn),[3b,7−9] group 15 (P, As),[10−13] and group 4 elements (Ti, Zr, Hf).[14,15] In 1995 we reported the first [1]ferrocenophanes bridged by group 16 (S, Se)[16,17] elements. The sulfur-bridged species **3** possesses a tilt angle of 31°, at that time the largest tilt-angle known. Incorporation of first row elements with smaller covalent radii would be expected to give rise to even more strained and tilted structures. With this in mind, we briefly reported the synthesis of the first boron-bridged [1]ferrocenophanes.[18,19] We report here full details of our work on the synthesis, structural characterization, novel reactivity, and polymerization behavior of these species. We also discuss the electronic structures of these unique molecules, which were investigated by means of UV−vis spectroscopy and theoretical calculations.

Results and Discussion

Synthesis and Characterization of Boron-Bridged [1]-Ferrocenophanes 4a−c. Reaction of dilithioferrocene·*n*TMEDA with aminodichloroboranes such as Me_2NBCl_2, $Me(Ph)NBCl_2$, and $nBu(Me)NBCl_2$ led to the formation of products that were insoluble in common organic solvents. The use of dichloroboranes with sterically demanding π-donor substituents on boron, specifically, aminodichloroboranes with bulky substituents on nitrogen, on the other hand resulted in the formation of the novel boron-bridged [1]ferrocenophanes **4a−c**.

Scheme 1. Synthesis of Boron-Bridged [1]Ferrocenophanes [**4a** (R = R′ = $SiMe_3$), **4b** (R = $SiMe_3$, R′ = *t*Bu), and **4c** (R = R′ = *i*Pr)]

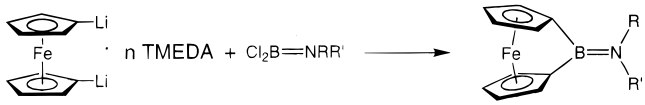

4

Slow addition of the aminodichloroboranes Cl_2BNRR' (R = R′ = $SiMe_3$; R = $SiMe_3$, R′ = *t*Bu; R = R′ = *i*Pr) to a slurry of dilithioferrocene·*n*TMEDA in hexanes or benzene at room temperature gave the boron-bridged [1]ferrocenophanes **4a−c** (Scheme 1). The ferrocenophanes were purified by recrystallization from hexanes followed by high vacuum sublimation and were obtained as dark red crystals in moderate yields of 35, 44, and 38%, respectively.

Characterization by ^1H, ^{13}C, and ^{11}B NMR, mass spectrometry, elemental analysis, and X-ray diffraction (**4a**, **4c**) confirmed the assigned structures. The ^1H NMR spectra show the characteristically large separation (**4a**, $\Delta\delta = 0.50$ ppm; **4b**, $\Delta\delta = 0.50$ ppm; **4c**, $\Delta\delta = 0.39$ ppm) of the signals assigned to the α and β Cp protons. In the ^{13}C NMR spectrum the signal of the *ipso*-C atom is found at δ 45.0 for **4a**, 45.2 for **4b**, and 44.2 for **4c** and is thus upfield shifted in comparison to unstrained systems (ferrocene, δ 68 ppm). However, with respect to the sulfur-bridged analogue (δ 14.3 ppm) or other less-strained [1]ferrocenophanes,[8,11−13,17] the signal appears at significantly lower field as a result of the electropositive nature of the bridging boron atom. The ^{11}B NMR signals are found at 48.3 (**4a**), 44.7 (**4b**), and 40.0 ppm (**4c**), and thus follow the trend in chemical shifts observed for the aminodichloroborane precursor molecules.[20]

X-ray Structures of Boron-Bridged [1]Ferrocenophanes 4a and 4c. To completely characterize and probe the strain present in **4**, single-crystal X-ray diffraction studies on **4a** and **4c** were undertaken. Crystals of compound **4c** contained two independent molecules in the unit cell. The crystal structures indicated that molecules of **4a** and **4c** are highly strained with tilt-angles of 32.4(2)° (**4a**) and 31.0(2)° and 31.4(2)° (**4c**) (Figures 1−3; Table 1). The tilt angle in **4a** represents the largest reported to date for an [*n*]ferrocenophane. The molecular structures of **4a** and **4c** are interesting to compare with that of the sulfur-bridged ferrocenophane **3**,[17] which exhibits a similar tilt angle of 31.1(1)°. The large ring tilting in **4a** and **4c** is accompanied by RC1−Fe−RC2 angles (RC = ring centroid) of 155.2(2)° (**4a**) and 155.9(2)° and 156.1(2)° (**4c**), which are slightly smaller than that in **3** (E = S) [156.9(1)°]. However, the angles β between the cyclopentadienyl ring planes and the exocyclic C−B bonds of 33.7(2)° and 34.0(2)° in **4a** and 35.3(3)°, 35.6(3)°, 34.3(3)°, and 36.1(3)° in **4c** are significantly larger than the β angles of 29.1(1)° and 28.8(1)° in **3**. This effect can be attributed to the different geometric features of the two bridging units. The boron atom adopts a trigonal planar configuration in which the angles between the three substituents are expected to be 120°, whereas for the bridging sulfur atom an angular geometry with an angle of about 109° is expected (C−S−C angle found for para-substituted diphenylsulfides[21]). However, the strain in **4a** and **4c** results in angles C(1)−B−

(8) Jäkle, F.; Rulkens, R.; Zech, G.; Foucher, D. A.; Lough, A. J.; Manners, I. *Chem. Eur. J.* **1998**, *4*, 2117.
(9) Sharma, H. K.; Cervantes-Lee, F.; Mahmoud, J. S.; Pannell, K. H. *Organometallics* **1999**, *18*, 399.
(10) Stoeckli-Evans, H.; Osborne, A. G.; Whiteley, R. H. *J. Organomet. Chem.* **1980**, *194*, 91.
(11) Osborne, A. G.; Whiteley, R. H.; Meads, R. E. *J. Organomet. Chem.* **1980**, *193*, 345.
(12) Seyferth, D.; Withers, H. P. *Organometallics* **1982**, *1*, 1275.
(13) Butler, I. R.; Cullen, W. R.; Einstein, F. W. B.; Rettig, S. J.; Willis, A. J. *Organometallics* **1983**, *2*, 128.
(14) Broussier, R.; Da Rold, A.; Gautheron, B.; Dromzee, Y.; Jeannin, Y. *Inorg. Chem.* **1990**, *29*, 1817.
(15) Broussier, R.; Da Rold, A.; Gautheron, B. *J. Organomet. Chem.* **1992**, *427*, 231.
(16) Pudelski, J. K.; Gates, D. P.; Rulkens, R.; Lough, A. J.; Manners, I. *Angew. Chem., Int. Ed. Engl.* **1995**, *34*, 1506.
(17) Rulkens, R.; Gates, D. P.; Balaishis, D.; Pudelski, J. K.; McIntosh, D. F.; Lough, A. J.; Manners, I. *J. Am. Chem. Soc.* **1997**, *119*, 10976.
(18) Braunschweig, H.; Dirk, R.; Müller, M.; Nguyen, P.; Resendes, R.; Gates, D. P.; Manners, I. *Angew. Chem., Int. Ed. Engl.* **1997**, *36*, 2338.
(19) For other boron-bridged [*n*]metallocenophanes see: (a) Braunschweig, H.; von Koblinski, C.; Wang, R. *Eur. J. Inorg. Chem.* **1999**, 69. (b) Braunschweig, H.; von Koblinski, C.; Mamuti, M.; Englert, U.; Wang, R. *Eur. J. Inorg. Chem.* **1999**, 1899. (c) Ashe, A. J., III.; Fang, X.; Kampf, J. W. *Organometallics* **1999**, *18*, 2288. (d) Stelck, D. S.; Shapiro, P. J.; Basickes, N.; Rheingold, A. L. *Organometallics* **1997**, *16*, 4546. (e) Rufanov, K.; Avtomonov, E.; Kazennova, N.; Kotov, V.; Khvorost, A.; Lemenovskii, D.; Lorberth, J. *J. Organomet. Chem.* **1997**, *536*, 361. For related boron-containing [*n*]ferrocenophanes see: (f) Herberhold, M.; Dörfler, U.; Milius, W.; Wrackmeyer, B. *J. Organomet. Chem.* **1995**, *492*, 59. (g) Herberhold, M.; Dörfler, U.; Wrackmeyer, B. *J. Organomet. Chem.* **1997**, *530*, 117. (h) Jäkle, F.; Priermeier, T.; Wagner, M. *J. Chem. Soc., Chem. Commun.* **1995**, 1765. (i) Jäkle, F.; Mattner, M.; Priermeier, T.; Wagner, M. *J. Organomet. Chem.* **1995**, *502*, 123.
(20) Nöth, H.; Wrackmeyer, B. *NMR, Basic Principles and Progress*; Diel, P., Fluck, E., Eds.; Springer-Verlag: Berlin, Heidelburg, New York, 1978; Vol. 14.
(21) Blackmore, W. R.; Abrahams, S. C. *Acta Crystallogr.* **1955**, *8*, 329.

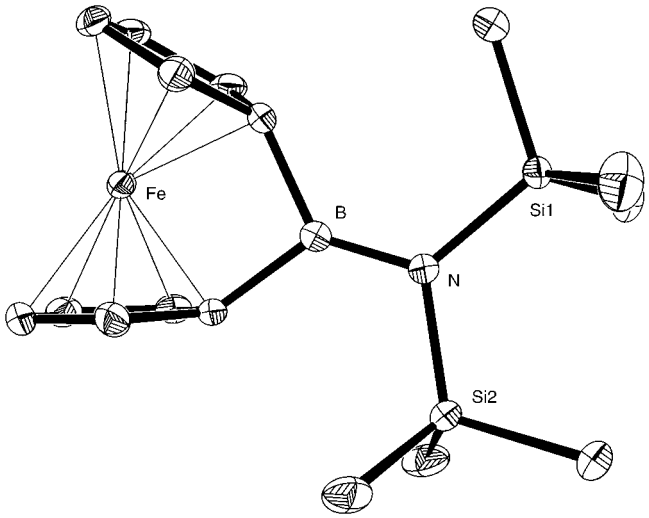

Figure 1. Molecular structure of **4a** with thermal ellipsoids at the 30% probability level.

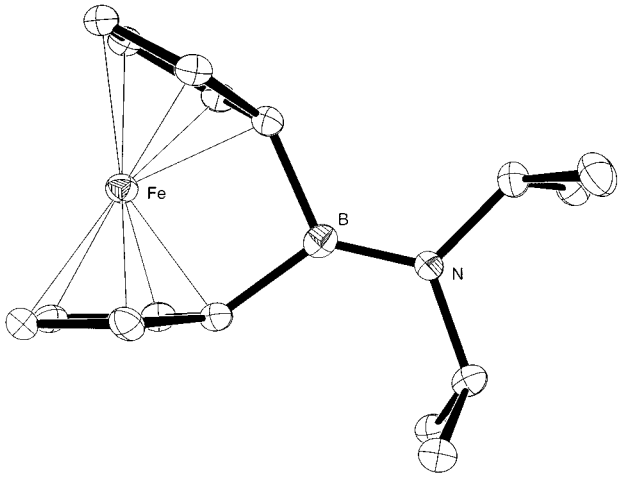

Figure 2. Molecular structure of $\mathbf{4c_A}$ with thermal ellipsoids at the 30% probability level.

C(6) of only 100.1° (**4a**) and 102.0(3)° and 103.2(3)° (**4c**), whereas an angle of 89.03(9)° is found for **3**. Another important point is that the B−C bonds (average values: **4a**, 1.617 Å; **4c**, 1.605 Å) are shorter in comparison to the S−C bonds (average: 1.806(2) Å). As a consequence, the Fe−B distances of 2.590(2) Å in **4a** and of 2.559(5) and 2.538(5) Å in **4c** are shorter than the Fe−S distance in **3** (2.7947(7) Å). However, the Fe−B distance is significantly longer than for a single bond (in $CpFe(CO)_2BPh_2$, d(Fe−B) = 2.034(3) Å; in $(C_5Me_5)Fe(CO)_2BClNMe_2$, d(Fe−B) = 2.027(5) Å)[22,23] and longer than the sum of the covalent radii (2.15 Å),[24] suggesting that no significant interaction is present. The B−N bond lengths are 1.399(2) Å (**4a**) and 1.371(6) and 1.384(6) Å (**4c**), which is typical for a B−N double bond (1.41 Å).[25]

Electronic Structure of Boron-Bridged [1]Ferrocenophanes 4a−c. (a) UV−Vis Spectra of 4a−c. In hexanes, **4a**, **4b**, and **4c** exhibit UV−vis absorbances at 479, 489, and 498 nm, respectively, which is considerably red-shifted with respect to ferrocene (λ_{max} = 440 nm). Replacement of the silyl substituents on nitrogen with alkyl substituents leads to a slight transition energy decrease. However, the absorbances are not as low energy as that for the sulfur-bridged [1]ferrocenophane **3** (λ_{max} = 504 nm). Therefore, the weakening of the iron−cyclopentadienyl bond, which decreases the HOMO-LUMO energy difference and therefore increases λ_{max}, seems to be not only related to the degree of ring tilting[17,26] but, in this case, appears to be influenced by subtle changes in the electronic surrounding of the bridging atom.

(b) DFT Calculations on 4a and 3. (i) Structure. To obtain deeper insight into the relationship between the structural and electronic properties of the [1]ferrocenophanes, DFT calculations were performed on both **4a** and the sulfur-bridged species **3**. A geometry optimization of **4a** and **3** assuming C_{2v} symmetry gave the theoretical (th) structural parameters summarized in Table 1. The calculated inter-ring angles α are found to be similar for the two compounds ($\mathbf{4a_{th}}$, 30.1°; $\mathbf{3_{th}}$, 30.7°) and are in fairly good agreement with the experimentally determined values. In the calculated structure of **4a** a slightly lower degree of ring tilting α results in a higher value for the β angle (**4a**, 33.7°, 34.0°; $\mathbf{4a_{th}}$, 38.9°). However, the major geometric differences between the two molecules, namely the shorter Fe−B distance in comparison to the Fe−S distance ($\mathbf{4a_{th}}$, 2.55 Å; $\mathbf{3_{th}}$, 2.82 Å), the shorter B−*ipso*C distance in comparison to the S-*ipso*C distance ($\mathbf{4a_{th}}$, 1.60 Å; $\mathbf{3_{th}}$, 1.83 Å), and the greater C−B−C angle in comparison to the C−S−C angle ($\mathbf{4a_{th}}$, 100.6°; $\mathbf{3_{th}}$, 88.7°) are reproduced in the calculated structures. Introduction of the smaller B atom, which would presumably prefer to adopt

Table 1. Selected Experimental and Calculated Bond Lengths [Å] and Angles [deg] for **4a**, **4c**, and **3**

	4a	$\mathbf{4a_{th}}$	$\mathbf{4c_A}$	$\mathbf{4c_B}$	**3**	$\mathbf{3_{th}}$
Fe−B/S	2.590(2)	2.55	2.559(5)	2.538(5)	2.7947(7)	2.82
Fe−C(1)	1.985	1.96	1.998(4)	1.987(4)	1.969(2)	1.98
Fe−C(2)	2.014	1.98	2.021(4)	2.021(4)	2.005(2)	2.02
Fe−C(3)	2.088	2.05	2.081(4)	2.087(4)	2.074(2)	2.10
Fe−C(4)	2.085	2.05	2.082(4)	2.077(4)	2.082(2)	2.10
Fe−C(5)	2.015	1.98	2.008(4)	2.007(4)	2.018(2)	2.02
Fe−C(6)	1.988	1.96	1.989(4)	1.992(4)	1.967(2)	1.98
Fe−C(7)	2.014	1.98	2.028(4)	2.011(4)	2.021(2)	2.02
Fe−C(8)	2.094	2.05	2.097(4)	2.076(4)	2.091(2)	2.10
Fe−C(9)	2.086	2.05	2.087(4)	2.079(4)	2.083(2)	2.10
Fe−C(10)	2.007	1.98	2.013(4)	2.015(4)	2.010(2)	2.02
C(1)−C(2)	1.446	1.45	1.447(5)	1.474(6)	1.439	1.45
C(2)−C(3)	1.433	1.43	1.422(5)	1.426(6)	1.420	1.43
C(3)−C(4)	1.418	1.42	1.422(5)	1.414(5)	1.419	1.42
C(4)−C(5)	1.430	1.43	1.415(5)	1.407(6)	1.418	1.43
C(5)−C(1)	1.450	1.45	1.442(5)	1.449(5)	1.442	1.45
C(6)−C(7)	1.448	1.45	1.462(5)	1.448(5)	1.445	1.45
C(7)−C(8)	1.429	1.43	1.419(6)	1.419(5)	1.419	1.43
C(8)−C(9)	1.415	1.42	1.429(5)	1.410(6)	1.417	1.42
C(9)−C(10)	1.425	1.43	1.414(6)	1.424(6)	1.425	1.43
C(10)−C(6)	1.446	1.45	1.450(5)	1.441(5)	1.446	1.45
B−N	1.399(2)	1.40	1.371(6)	1.384(6)		
B/S−C(1)	1.611	1.60	1.623(6)	1.597(6)	1.807(2)	1.83
B/S−C(6)	1.624	1.60	1.597(6)	1.604(6)	1.805(2)	1.83
C(1)−B-N	131.8	129.7	127.0(4)	127.0(4)		
C(6)−B-N	128.1	129.7	131.0(4)	129.7(4)		
C(1)−B/S−C(6)	100.1	100.6	102.0(3)	103.2(3)	89.03(9)	88.7
B−N−Si(1)/C(11)	123.0	115				
B−N−Si(2)/C(14)	115.5					
α	32.4(2)	30.1	31.4(2)	31.0(2)	31.1(1)	30.7
β	33.7(2)	38.9	35.3(3)	34.3(3)	29.1(1)	28.9
	34.0(2)		35.6(3)	36.1(3)	28.8(1)	

(22) Braunschweig, H.; Kollann, C.; Englert, U. *Eur. J. Inorg. Chem.* **1998**, 465.

(23) For other references on transition metal boryl compounds see: (a) Irvine, G. J.; Lesley, M. J. G.; Marder, T. B.; Norman, N. C.; Rice, C. R.; Robins, E. G.; Roper, W. R.; Whittell, G. R.; Wright, L. J. *Chem. Rev.* **1998**, *98*, 2685. (b) Braunschweig, H. *Angew. Chem., Int. Ed. Engl.* **1998**, *37*, 1786. (c) He, X.; Hartwig, J. F. *Organometallics* **1996**, *15*, 400. (d) Hartwig, J. F.; Huber, S. *J. Am. Chem. Soc.* **1993**, *115*, 4908.

(24) Huheey, J. E.; Keiter, E. A.; Keiter, R. L. *Inorganic Chemistry*; Harper Collins: New York, 1993.

(25) Paetzold, P. *Adv. Inorg. Chem.* **1987**, *31*, 123; see p 137.

(26) Barlow, S.; Drewitt, M. J.; Dijkstra, T.; Green, J. C.; O'Hare, D.; Whittingham, C.; Wynn, H. H.; Gates, D. P.; Manners, I.; Nelson, J. M.; Pudelski, J. K. *Organometallics* **1998**, *17*, 2113.

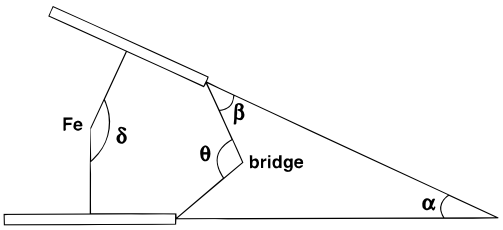

Figure 3. Key structural parameters for [1]ferrocenophanes.

a 120° angle, results in greater strain shown by the reduction of the angle at the bridge to 100.6°. The Cp rings on the other hand do not bend further since the cost of bending increases at a faster rate with an increase in bending angle as shown by DFT calculations on ferrocene.[26,27]

(ii) Orbital Energies. The calculated orbital and excitation energies are summarized in Table 2. Generally, the d orbitals are higher in energy in **4a$_{th}$** than in **3$_{th}$**. Interestingly, the orbitals associated with the bridge are in a different position in the energy manifold for **4a$_{th}$** than for **3$_{th}$**. The equivalent of the sulfur p lone pair, which in **3$_{th}$** is higher in energy than the Fe−Cp bonding orbitals, is the B−N π bond, which in the case of **4a$_{th}$** lies among the Fe−Cp bonding orbitals. The B−N π bond mixes hyperconjugatively with the Si−C bonds. The B−C b_2 bonding orbital lies higher in energy than the S−C bonds, which are below the Fe−Cp bonding orbitals in the energy manifold of **3$_{th}$**. The B−C b_2 bonding orbital on the other hand lies in a similar energy region as the Fe−Cp bonding orbitals and mixes strongly with the Fe−Cp b_2 bonding orbital. The B−C a_1 interaction lies lower in energy, stabilized by mixing with the N pσ orbital.

The order of the two highest occupied orbitals, which are very close in energy, is reversed. In **4a$_{th}$** the HOMO is a_1, whereas in **3$_{th}$** it is b_1 in symmetry. In comparison, the HOMO for ferrocene that is bent to 30° is a_1 in symmetry and even more separated from the b_1 orbital than in **4a$_{th}$**.[27] The reversed order in **3$_{th}$** may be a consequence of interaction with the bridge p orbital of b_1 symmetry. There is also a change in LUMO between **4a$_{th}$** and **3$_{th}$**. In **3$_{th}$** it is an orbital of b_2 symmetry, which is the same as in bent unbridged ferrocene. In **4a$_{th}$** it has changed to the a_2 orbital. This effect may be attributed to mixing with the b_2 set of the bridge B−C orbitals.

The HOMO-LUMO gap is slightly larger in **4a$_{th}$** than **3$_{th}$**. This is due both to the raising of the b_1 d orbital in **3$_{th}$** and the raising of the empty $3b_2$ orbital in **4a$_{th}$**. In other words the calculations indicate that the HOMO-LUMO gap may be primarily affected by the inter-ring angle α but is also fine-tuned by the energy of the bridge orbitals.

(iii) Excitation Energies. The energies for excitations from the HOMO in **4a$_{th}$** to the first three unoccupied orbitals were calculated (Table 3). The prediction is that the first spin allowed band is at shorter wavelength in **4a$_{th}$** than in **3$_{th}$**[26] and may be attributed to an increase in the HOMO-LUMO gap. This is in line with the experimental observations for **4a** and **3** which is a satisfying result.

Reactivity of Boron-Bridged [1]Ferrocenophanes 4a−c: The Discovery of Unusual Fe−Cp Bond Cleavage Reactions. (a) Attempted Insertion and Ring-Opening Addition Reactions Involving the B−Cp Bond. Silicon-bridged [1]ferrocenophanes and other group 14 element-bridged [1]ferrocenophanes undergo insertion reactions with platinum compounds such as $Pt(COD)_2$ (COD = cyclooctadiene) or $Pt(PEt_3)_3$[28] to afford species such as **5**, and polymerize in the presence of catalytic amounts of Karstedt's catalyst or $PtCl_2$.[5c] In light of these observations, the reactivity of the boron-bridged compounds **4** toward these reagents was also investigated. However, the attempted equimolar reaction of $Pt(COD)_2$ with the boron-bridged species **4b** did not result in the formation of an insertion compound even at elevated temperatures (40 °C), and extended periods of time. Instead, gradual decomposition of the platinum compound, with production of COD, was observed in the NMR spectral data. Similarly, reaction with a catalytic amount of Karstedt's catalyst did not lead to ROP.

On the other hand, reaction of the boron-bridged [1]-ferrocenophane **4c** with MeOH and HCl, respectively, led to a complex mixture of products, which could not be identified or characterized. This contrasts with the reactivity found for silicon-bridged [1]ferrocenophanes, which upon treatment with MeOH or HCl selectively form the ring-opened monosubstituted ferrocenes **6** (X = OMe, Cl).[29,30]

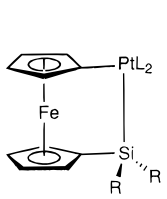

5

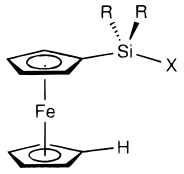

6

(b) Reactions with $Fe(CO)_5$ or $Fe_2(CO)_9$ and with $Co_2(CO)_8$. The reaction of the boron-bridged [1]ferrocenophanes **4** with metal carbonyl compounds was investigated to further explore the reactivity of these highly strained compounds.

(i) Photochemical Reaction with $Fe(CO)_5$. Photochemical reaction between **4c** and $Fe(CO)_5$ in THF at −30 °C led to the isolation of a dark red crystalline solid. The ^{11}B NMR spectrum of the product showed a singlet at δ 37.5, a region typical for aminodiorganylboranes.[31] The solution IR spectrum displayed two bands at $\bar{\nu}$ = 1781 and 1990 cm^{-1} for the carbonyl stretching modes which indicated the presence of bridging and terminal groups, respectively. Single-crystal X-ray diffraction showed the product to be **7**, the result of insertion of an iron carbonyl fragment into the Fe−Cp bond of **4c**. The molecular structure of **7** is shown in Figure 4 and selected bond lengths and angles are given in Table 4.

Compound **7** is a boron-bridged analogue of the well-known dimer $[Cp(CO)Fe(\mu\text{-}CO)]_2$, which indicated the insertion of a photochemically generated $Fe(CO)_4$ fragment into the Fe−Cp bond followed by rearrangement of the carbonyl ligands had taken place. An analogous silicon-bridged compound, $Fe_2[SiMe_2(\eta\text{-}C_5H_4)_2](CO)_4$, has previously been prepared from $Fe(CO)_5$ and $(C_5H_4)_2SiMe_2$ under reflux conditions.[32] The Fe−Fe distance of 2.499(1) Å in **7** is comparable to the Fe−Fe distance in *cis*-$[Cp(CO)Fe(\mu\text{-}CO)]_2$ (2.533 Å)[33] and to that of the silicon-bridged analogue (2.512(3) Å). The distance from the iron atoms to both the bridging (1.924(5), 1.935(5), 1.919-(5), 1.938(5) Å) and the terminal (1.747(4), 1.755(4) Å) carbonyl groups in **7** is also similar to the analogous distances in [Cp-

(27) Green, J. C. *J. Chem. Soc. Rev.* **1998**, *27*, 263.
(28) Sheridan, J. B.; Temple, K.; Lough, A. J.; Manners, I. *J. Chem. Soc., Dalton Trans.* **1997**, 711.
(29) Fischer, A. B.; Kinney, J. B.; Staley, R. H.; Wrighton, M. S. *J. Am. Chem. Soc.* **1979**, *101*, 6501.
(30) MacLachlan, M. J.; Ginzburg, M.; Zheng, J.; Knöll, O.; Lough, A. J.; Manners, I. *New J. Chem.* **1998**, 1409.
(31) Nöth, H.; Wrackmeyer, B. *Nuclear Magnetic Resonance Spectroscopy of Boron Compounds*, 14th ed.; Springer-Verlag KG: Berlin, Heidelberg, New York, 1978.
(32) Weaver, J.; Woodward, P. *J. Chem. Soc., Dalton Trans.* **1973**, 1439.
(33) Bryan, R. F.; Greene, P. T.; Field, D. S.; Newlands, M. J. *J. Chem. Soc., Chem. Commun.* **1969**, 1477.

Table 2. Calculated Orbital Energies (eV), Assigned Orbital Numbers, Symmetry, and Type for $\mathbf{4a_{th}}$ and $\mathbf{3_{th}}$

$\mathbf{4a_{th}}$			$\mathbf{3_{th}}$		
orbital energy	orbital no. and symmetry	orbital type[a]	orbital energy	orbital no. and symmetry	orbital type[a]
−1.19	$4b_1$	B−N π*	−0.99	$5a_1$	S−C (ab)
−1.35	$3b_2$	d−Cp (ab)	−1.78	$3a_2$	d−Cp (ab)
−1.39	$3a_2$(LUMO)	d−Cp (ab)	−1.83	$3b_2$(LUMO)	d−Cp (ab)
−4.11	$4a_1$(HOMO)	d	−4.40	$3b_1$(HOMO)	d
−4.29	$3b_1$	d	−4.43	$4a_1$	d
−4.73	$3a_1$	d	−4.94	$3a_1$	d
−6.23	$2a_1$	Cp−d (b)	−5.62	$2b_1$	S p
−6.33	$2b_1$	B−N π	−6.46	$2a_1$	Cp−d (b)
−6.43	$1b_1$	Cp−d (b)	−6.62	$1b_1$	Cp−d (b)
−6.48	$2b_2$	Cp−d and B−C (b)	−6.91	$2a_2$	Cp−d (b)
−6.68	$2a_2$	Cp−d (b)	−6.92	$2b_2$	Cp−d (b)
−6.92	$1b_2$	Si−C (b)	−8.39	$1a_1$	S−C (b)
−7.14	$1a_2$	Si−C (b)	−8.92	$1b_2$	S−C (b)
−7.17	$1a_1$	Si−C (b)			
−7.38	$0b_2$	Cp−d, B−C and N−Si (b)			
−7.96	$0b_1$				
−8.45	$-1b_2$				
−8.51	$0a_1$	B−C and B−N (b)			

[a] b and ab in parentheses stand for bonding and antibonding orbitals, respectively.

Table 3. Calculated Excitation Energies (eV) and Corresponding Wavelengths λ (nm), for $\mathbf{4a_{th}}$ and $\mathbf{3_{th}}$

	$\mathbf{4a_{th}}$		$\mathbf{3_{th}}$[a]	
excitation	energy (eV)	λ (nm)	energy (eV)	λ (nm)
$3b_2 \leftarrow 4a_1$	2.47	502	2.16	574
$3a_2 \leftarrow 4a_1$	2.66	466	2.48	501
$4b_1 \leftarrow 4a_1$	3.67	338		
$5a_1 \leftarrow 4a_1$			3.61	343

[a] For further details on the electronic transitions in $\mathbf{3_{th}}$ see ref 26, Table 5.

Scheme 2. Photochemical Reaction of **4c** with $Fe(CO)_5$ in THF

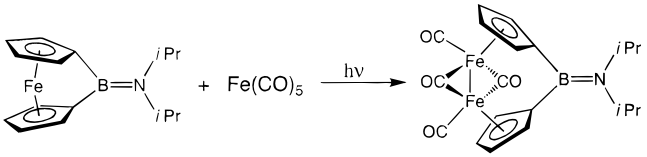

4c **7**

$(CO)Fe(\mu\text{-}CO)]_2$ (d(Fe-bridging CO) = 1.93 Å average; d(Fe-terminal CO) = 1.76 Å average). The B−N bond length (1.373(6) Å) in **7** is virtually unaltered from that in the boron-bridged [1]ferrocenophane precursor **4c** (average: 1.378 Å). In addition, the B−C bond lengths of the insertion products **7** (average: 1.589 Å) and **4c** (average: 1.617 Å) are similar. However, the RC(1)−Fe(1)−Fe(2) (126.6°) and RC(2)−Fe(2)−Fe(1) (126.9°) angles in **7** are smaller than those in *cis*-[Cp-$(CO)Fe(\mu\text{-}CO)]_2$ (135°), indicating that appreciable strain may still be present.

(ii) Reaction with $Fe_2(CO)_9$. Reaction of $Fe_2(CO)_9$ with the boron-bridged ferrocenophane **4c** in a 2:1 ratio in THF was also performed in an attempt to form **7** under more convenient conditions. Analysis of the ^{1}H NMR spectrum confirmed that **7** was the product formed in this alternate route, and no byproducts were detectable spectroscopically. In this case, the product was isolated in a 64% yield.

(iii) Reaction with $Co_2(CO)_8$. After mixing equimolar quantities of **4b** and $Co_2(CO)_8$ in C_6D_6 at 25 °C, no unreacted **4b** could be detected by ^{1}H NMR after 1 h. Solvent removal and recrystallization yielded a brown crystalline product. The ^{1}H NMR spectrum of this compound showed seven distinct signals in the region from 5.26 to 4.49 ppm assigned to protons

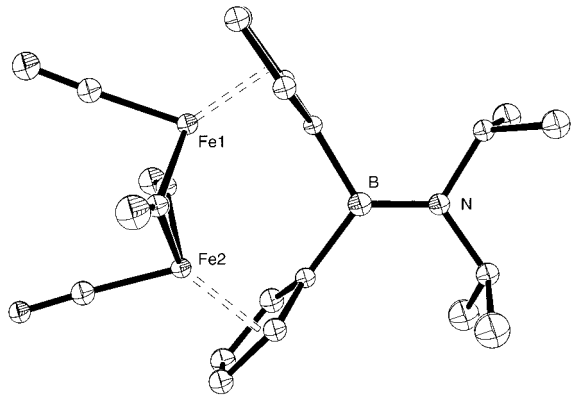

Figure 4. Molecular structure of **7** with thermal ellipsoids at the 30% probability level.

on the Cp rings. These resonances are considerably downfield shifted from those of **4b** (four resonances from 4.42 to 3.92 ppm). Similarly, the ^{13}C NMR spectrum of the product showed eight closely spaced peaks assigned to the non-*ipso* carbon atoms of the Cp rings (from 92.9 to 89.3 ppm), which are downfield-shifted with respect to those of **4b** (76.7−72.0 ppm). The increase in the number of resonances in the ^{1}H and ^{13}C NMR spectra for the Cp ligands indicated that the product has intrinsically less symmetrical structure than that of **4b**. The ^{11}B NMR spectrum of the product showed a single broad resonance at a chemical shift of 49.6 ppm, which is only slightly downfield-shifted in comparison to the resonance observed for **4b** (44.7 ppm). This again suggested that the B−Cp bonds were not cleaved. Single crystal X-ray diffraction was also used in this case to unequivocally determine the structure of the product. This showed that the compound was the novel trimetallic species **8**. The molecular structure is shown in Figure 5 and selected bond lengths and angles are given in Table 5. The product contains a $CpCo(CO)_2$ fragment, and a $Cp(CO)_2Fe-Co(CO)_4$ fragment linked by a boron bridge. The detailed mechanism of formation of **8** is not obvious, but clearly the reaction of **4b** with $Co_2(CO)_8$ leads to insertion into the iron−Cp bond, which is presumably followed by the redistribution of carbonyl groups.

The Fe−Co bond distance (2.7152(4) Å) in **8** is significantly longer than that of the known heterodimer $Cp(CO)Fe(\mu\text{-}CO)_2Co(CO)_3$, which has an Fe−Co bond distance of 2.545(1)

Table 4. Selected Bond Lengths [Å] and Angles [deg] for **7**

Fe(1)−Fe(2)	2.4987(8)	O(3)−C(3)	1.182(6)	Fe(2)−Fe(1)−C(1)	107.0(1)
Fe(1)−C(1)	1.747(4)	O(4)−C(4)	1.167(6)	Fe(2)−Fe(1)−C(3)	49.4(1)
Fe(1)−C(3)	1.924(5)	N−B	1.373(6)	Fe(2)−Fe(1)−C(4)	49.9(1)
Fe(1)−C(4)	1.935(5)	C(10)−B	1.589(6)	Fe(1)−C(1)−O(1)	177.8(4)
Fe(2)−C(2)	1.755(4)	C(20)−B	1.588(6)	Fe(2)−C(2)−O(2)	177.9(4)
Fe(2)−C(3)	1.919(5)	N−B−C(20)	121.1(4)	C(31)−N−C(34)	113.8(3)
Fe(2)−C(4)	1.938(5)	N−B−C(10)	125.4(4)	Fe(1)−C(3)−Fe(2)	81.1(2)
Fe(2)−C(20)	2.143(4)	N−B−C(31)	120.9(4)	Fe(1)−C(4)−Fe(2)	80.4(2)
O(1)−C(1)	1.148(5)	N−B−C(34)	125.3(4)	Fe(2)−C(3)−O(3)	140.7(4)
O(2)−C(2)	1.145(5)	C(10)−B−C(20)	113.6(4)	Fe(2)−C(4)−O(4)	139.1(4)

Scheme 3. Room Temperature Reaction of **4b** with $Co_2(CO)_8$ in C_6D_6

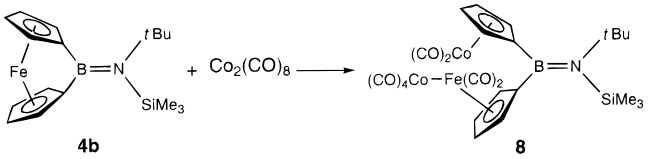

Å.[34] However, in contrast to the latter compound, **8** contains no bridging carbonyls in the solid state. The Fe−Co distance of **8** is similar to that of $CpFe(\mu\text{-PNP})_2Co(CO)_2$ (PNP = MeN-$(PF_2)_2$) (2.743(1) Å), for which a covalent Fe−Co interaction was discussed although the Fe−Co distance is longer than the average distances found in binuclear and cluster compounds (2.45−2.67 Å).[35] The solution IR spectrum of **8** on the other hand showed a variety of bands in the regions characteristic of terminal *and* bridging carbonyl groups, which suggests the presence of a mixture of structural isomers as observed for Cp-$(CO)Fe(\mu\text{-CO})_2Co(CO)_4$.[36]

Ring-Opening Polymerization of Boron-Bridged [1]Ferrocenophanes 4a−c. To explore the thermal polymerization behavior of monomers **4a**−**c**, a Differential Scanning Calorimetry (DSC) study was undertaken (Figure 6, Table 6). The DSC thermogram of **4a** showed a melt endotherm at approximately 115 °C (onset), followed by a ROP exotherm (vide infra) at about 200 °C (onset). The enthalpy for the ROP of **4a** was determined to be 95 kJ mol^{-1}. This value is greater than the ROP enthalpy for silicon-bridged [1]ferrocenophanes (70−80 kJ mol^{-1}),[37] which possess smaller tilt-angles (16−21°),[37] but is substantially less than for the sulfur-bridged [1]ferrocenophane **3** (ca. 130 kJ mol^{-1}), which has a slightly smaller tilt-angle (31°).[17] The substantial difference in the ROP enthalpy for **4a** and **3** is most likely a consequence of the difference in steric bulk between the bridging moieties. Side group interactions between sterically demanding substituents generally cause substantial destabilization of polymers relative to monomers which leads to dramatic decreases in polymerization enthalpy. In the case of **4a** a bulky amino substituent is attached to the bridging atom whereas no substituents are present at all in the case of **3**. Studies of a sterically unencumbered boron-bridged [1]ferrocenophane, which has not yet been synthesized, would therefore be needed to permit a realistic comparison of intrinsic ring-strain with other [1]ferrocenophanes such as **3**.

The DSC thermogram of compound **4b** showed a melt endotherm at ca. 150 °C (onset) overlapping with the ROP exotherm at only slightly higher temperature. A similar DSC thermogram was found for **4c,** which shows a melt endotherm at ca. 185 °C overlapping with a ROP exotherm. It can be concluded that the melting points for **4a**−**c** are strongly influenced by the substituents on nitrogen; introduction of trimethylsilyl for alkyl substituents on nitrogen lowers the melt transition temperature. The ROP exotherm on the other hand is found at very similar temperatures for all three of the bora[1]-ferrocenophanes **4**a−**c**.

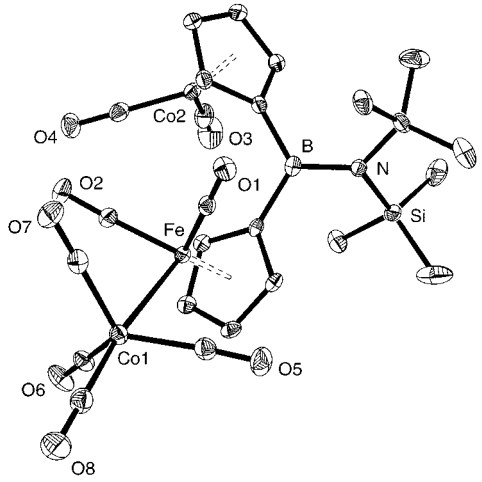

Figure 5. Molecular structure of **8** with thermal ellipsoids at the 30% probability level.

The products obtained from thermal polymerization of **4a** (180 °C; 2 h in a sealed, evacuated, Pyrex tube) were found to be mainly insoluble in organic solvents. An ^1H NMR spectrum of the minor soluble fraction in C_6D_6 shows three different sets of signals, none of which can be assigned to the monomer **4a**. However, one set of signals (δ 4.26, 4.66, 0.33 ppm) can be attributed to a cyclic dimer ($n = 2$) by comparison with an independently synthesized sample.[38] Accordingly, the pyrolysis mass spectrum of the product mixture showed molecular ions for several ferrocenylborane oligomers ($n = 1, 2, 3$) (Scheme 4). The insoluble fraction, **9a**, was isolated as a bright red powder, and to gain further insight into the structure of this material, solid state ^{13}C NMR spectroscopy was performed. Resonances at δ 77.6 and 74.1 ppm in the Cp region (**4a** = 77.1, 72.4 ppm) and a resonance at 5.1 ppm corresponding to the $SiMe_3$ groups of the aminoborane functionality were observed. The product obtained from heating **4b** to 200 °C for 3 h was found to be completely insoluble in organic solvents. However, thermal polymerization of **4c** (200 °C; 1 h) gave a material that was almost completely soluble in polar organic solvents such as toluene, THF, CH_2Cl_2, or chloroform. Mass spectrometric analysis of the crude product suggested the presence of cyclic dimeric and trimeric ferrocenylborane oli-

(34) Campbell, I. L. C.; Stephens, F. S. *J. Chem. Soc., Dalton Trans.* **1975**, 22.

(35) Mague, J. T.; Lin, Z. *Organometallics* **1992**, *11*, 4139. However, it should be noted that there is a difference of 2 in the electron count for compound **8** and $CpFe(PNP)_2Co(CO)_2$.

(36) Manning, A. R. *J. Chem. Soc. (A)* **1971**, 2321.

(37) Pudelski, J. K.; Foucher, D. A.; Honeyman, C. H.; Lough, A. J.; Manners, I.; Barlow, S.; O'Hare, D. *Organometallics* **1995**, *14*, 2470.

(38) The boron-bridged cyclic dimers were synthesized via the reaction of $FeCl_2$ with $Li_2[(C_5H_4)_2BNR_2]$: Braunschweig, H.; von Koblinski, C. Unpublished results.

Table 5. Selected Bond Lengths [Å] and Angles [deg] for **8**

Fe(1)−Co(1)	2.7152(4)	Co(1)−C(17)	1.812(3)	B(1)−C(1)	1.580(4)
Fe(1)−C(11)	1.768(3)	Co(1)−C(18)	1.786(3)	B(1)−C(6)	1.559(4)
Fe(1)−C(12)	1.773(2)	Co(2)−C(13)	1.741(3)	C(1)−B−C(6)	121.1(2)
Co(1)−C(15)	1.782(3)	Co(2)−C(14)	1.739(3)	C(18)−Co(1)−Fe(1)	172.5(1)
Co(1)−C(16)	1.801(3)	B(1)−N(1)	1.440(3)	C(13)−Co(2)−C(14)	91.4(1)

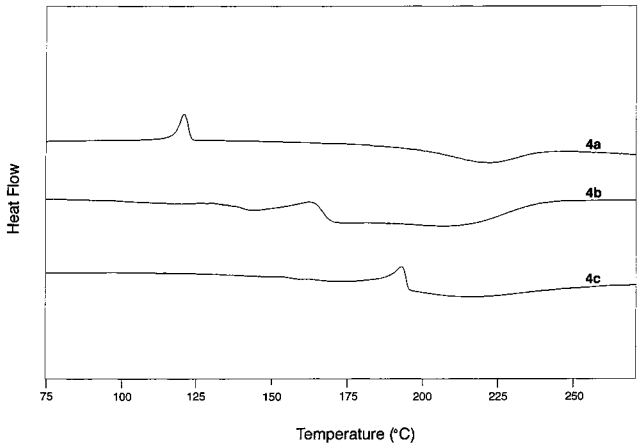

Figure 6. DSC thermograms of **4a**−**c** (heating rate = 10 °C/min, under N_2).

Table 6. Comparison of DSC Results for the Thermal ROP of Compounds **4a**, **4b**, and **4c** with Onset Temperatures Given

compound	**4a**	**4b**	**4c**
mp [°C]	115	150[a]	185[a]
ROP [°C]	200	ca. 170−220	ca. 170−200[a]
ΔH ROP [kJ mol^{-1}]	−95	a	a

[a] For **4b** and **4c** the melt transition is overlapping with the ROP exotherm, therefore accurate values for the ROP enthalpy could not be determined.

Scheme 4. Thermal Polymerization of **4** [**4a**, 180 °C; **4b**, 200 °C; **4c**, 200 °C] To Yield **9** [**9a** (R = R′ = $SiMe_3$), **9b** (R = *t*Bu; R′ = $SiMe_3$), **9c** (R = R′ = *i*Pr)]

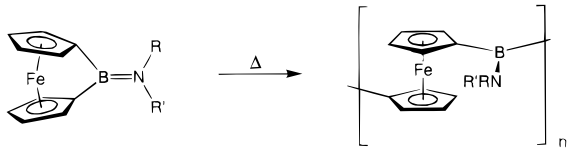

4 **9**

gomers (n = 2, 3). An NMR spectroscopic investigation of the same crude product mixture revealed the formation of three products. A cyclic dimeric structure could be assigned to one minor component by comparison with an independently synthesized sample,[38] and the other minor component was assigned a trimeric structure from the previously mentioned mass spectral data. The major component, **9c** (ca. 50% by ^{1}H NMR integration), of the mixture was isolated in pure form via precipitation from toluene into dry hexanes. The ^{11}B NMR spectrum of **9c** showed a signal at δ 41.5 ppm, which is only slightly upfield shifted in comparison to the monomer **4c** (δ 40.0 ppm). However, the ^{1}H NMR spectrum differs significantly from that of both monomer and cyclic dimer/trimer. Most significantly, the CH protons and the methyl groups for the isopropyl groups are strongly downfield shifted (δ 5.42, 1.41 ppm) in comparison to **4c** (δ 3.84, 1.20 ppm). This assignment was confirmed by two-dimensional NMR techniques (COSY, HSQC, HMBC). For example, a cross-peak between the *i*Pr tertiary carbon atom (50.6 ppm) and the proton at 5.42 ppm was observed in the HSQC spectrum (see Figure 7 for the HSQC spectrum of **9c**). The

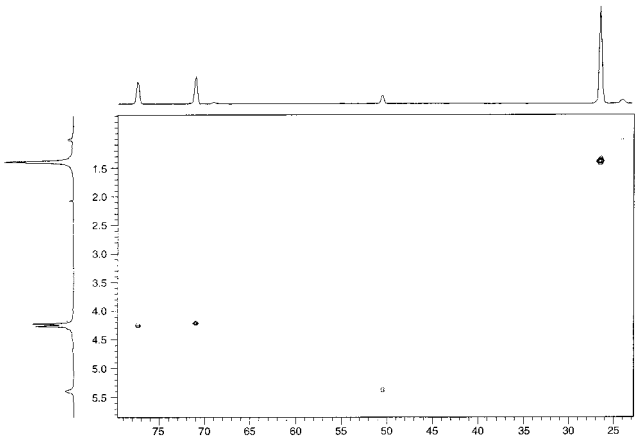

Figure 7. (^{1}H/^{13}C) HSQC spectrum of **9c** (C_6D_6, 20 °C).

COSY spectrum showed a cross-peak between the CH proton of the *i*Pr functionality and the protons of the associated methyl groups (1.41 ppm). Furthermore, the splitting of the two Cp resonances is much smaller than that in **4c** ($\Delta\delta$ 0.04 ppm; **4c**, 0.39 ppm) which, in similar poly(ferrocene) systems, is indicative of the formation of polymeric material.

Analysis of the molecular weight of the poly(boraferrocene) **9c** by conventional techniques (e.g. gel permeation chromatography) was not possible due to the hydrolytic sensitivity of this material. Dynamic light scattering studies of a toluene solution of **9c** under nitrogen showed no detectable signal, which indicated that the polymer possessed a hydrodynamic radius (R_H) < 2.3 nm. This is consistent with the presence of low molecular weight material. For comparison, the M_n value for poly(ferrocenyldimethylsilane) **2** (ER_x = $SiMe_2$) with R_H = ca. 2.3 nm is around 9000.[39]

TGA analysis of **4** in the temperature range from 30 to 900 °C shows that above the polymerization temperatures significant weight loss occurs. For example, in the case of **4c** a sharp weight loss of ca. 50% is observed in the temperature range from 200 to 400 °C followed by a slower decrease in weight. After heating to 900 °C, a black powdery material is obtained in 23% yield.

Summary

Reaction of dilithioferrocene·*n*TMEDA with aminodichloroboranes has given the first boron-bridged [1]ferrocenophanes **4a**−**c**. Single-crystal X-ray analyses of **4a** and **4c** show tilt-angles between the planes of the Cp rings of 31−32°, which are the largest reported to date for an [*n*]ferrocenophane. The UV−vis spectra reveal a considerable redshift of the lowest energy absorbances in comparison to that of ferrocene but the absorbances are not as low energy as that for the sulfur-bridged [1]ferrocenophane **3**, which shows a slightly smaller Cp ring tilt angle. This observation suggests that in addition to ring-tilting, the electronic nature of the bridging element influences the HOMO-LUMO gap in strained [1]ferrocenophanes. A comparative investigation of the electronic structures of **4a** and **3** using DFT calculations confirmed that this is the case, and

(39) Massey, J.; Kulbaba, K.; Manners, I.; Winnik, M. Unpublished results.

revealed that the HOMO-LUMO gap is indeed slightly larger in **4a** than **3**.

The boron-bridged [1]ferrocenophanes readily undergo unprecedented ring-opening reactions with transition metal carbonyls. Insertion of fragments derived from $Fe(CO)_5$, $Fe_2(CO)_9$, and $Co_2(CO)_8$ occurs into the Fe−Cp bond forming **7**, a novel boron-bridged analogue of *cis*-$[CpFe(CO)_2]_2$, and the trimetallic $FeCo_2$ species **8**. Monomers **4a** and **4b** undergo thermal ROP to give the insoluble poly(ferrocenylboranes) **9a** and **9b**, respectively, together with small amounts of cyclic dimers and trimers. In the case of **4c**, the soluble poly(boraferrocene) **9c** was formed. Although the hydrolytic sensitivity of this material prevented accurate molecular weight analysis, the polymer was shown to be of low molecular weight by dynamic light scattering.

We believe it likely that higher molecular weight analogues of **9c** will be accessible by ROP if boron-bridged [1]ferrocenophanes with smaller substituents at boron can be prepared. Such species are current synthetic targets in our program as are species with ligation that might lead to hydrolytically stable ring-opened polymeric materials whose properties could then be studied in detail.

Experimental Section

Computational Methods. Calculations were performed using density functional methods of the Amsterdam Density Functional package (Version 2.3).[40] The electronic configurations were described by an uncontracted triple-ζ basis set of Slater type orbitals, with a single polarization functional added to the main group elements: 2p on hydrogen and 3d on carbon and boron atoms. The cores of the atoms were frozen, carbon and boron up to the 1s, and iron to 2p. Energies were calculated using Vosko, Wilk, and Nusair's local exchange correlation,[41] with nonlocal-exchange corrections by Becke,[42] and nonlocal correlation corrections by Perdew.[43] The nonlocal correction terms were not utilized in calculating gradients during geometry optimizations. This has been shown to be computationally efficient and improves metal−ligand bond distances.[44]

Experimental Details. The compounds BCl_3, *i*Pr_2NH, *t*Bu$(SiMe_3)NH$, $(SiMe_3)_2NH$, TMEDA, $Co_2(CO)_8$, $Fe(CO)_5$, and $Fe_2(CO)_9$ were purchased from Aldrich. Karstedt's catalyst (xylenes solution) was obtained from Gelest. The amines were distilled from CaH_2 prior to use. Dilithioferrocene·*n*TMEDA,[45] Cl_2BNiPr_2,[46] $Cl_2BN(tBu)SiMe_3$,[47] $Cl_2BN(SiMe_3)_2$,[48] $Cl_2BN(Me)Bu$,[46] and $Cl_2BN(Me)Ph$[46] were synthesized according to literature procedures. All reactions and manipulations were carried out under an atmosphere of prepurified nitrogen using either Schlenk techniques or an inert-atmosphere glovebox. Solvents were dried by standard methods and were distilled and stored over molecular sieves prior to use. The irradiation experiment was carried out through use of a Hereaus TQ 150 high-pressure Hg lamp. 200, 300, or 400 MHz ^{1}H NMR spectra were recorded on either a Varian Gemini 200, a Varian Gemini 300, or a Varian Unity 400 spectrometer. ^{13}C NMR spectra were recorded on a Varian Gemini 300 spectrometer (75.5 MHz) or a Varian Unity 400 spectrometer (100.4 MHz), ^{11}B NMR spectra (160.4 MHz) were recorded on a Varian Unity 500 spectrometer, and ^{29}Si NMR spectra (79.3 MHz) were recorded on a Varian Unity 400 spectrometer. Two-dimensional NMR experiments were carried out on a Varian Unity 500 spectrometer. All solution ^{1}H and ^{13}C NMR spectra were referenced internally to protonated solvent shifts. ^{11}B NMR spectra were referenced externally to BF_3·OEt_2. Solid-state NMR spectra were obtained on a Bruker DSX-400 (^{13}C at 100.6 MHz) spectrometer and were referenced to adamantane (^{13}C, 38.4 ppm vs TMS). UV−vis spectra were obtained using a Perkin-Elmer Lamda 900 UV−vis/near-IR spectrophotometer in hexanes at concentrations of 1.0 mmol L^{-1}. Mass spectra were obtained with the use of a VG 70−250S mass spectrometer operating in Electron Impact (EI) mode. The calculated isotopic distribution for each ion was in agreement with experimental values. The thermal behavior of the boron-bridged monomers and polymers was studied using a Perkin-Elmer DSC-7 differential scanning calorimeter equipped with a TAC-7 instrument controller. Thermograms were calibrated with the melt transitions of hexane and indium and were obtained at a heating rate of 10 °C/min under a nitrogen atmosphere. Thermogravimetric analyses (TGA) were performed using a Perkin-Elmer TGA-7 analyzer under nitrogen at a heating rate of 10 °C/min. Dynamic light scattering experiments were carried out on a wide angle laser light scattering photometer from Brookhaven Instruments Corporation using a 5-mW vertically polarized He−Ne laser as the light source. Details of this procedure are described elsewhere.[49] Elemental analyses were performed by Quantitative Technologies, Inc., Whitehouse, NJ.

Reaction of Dilithioferrocene·*n*TMEDA with $[(Me_3Si)_2N]BCl_2$: $Fe(\eta^5\text{-}C_5H_4Li)_2$·TMEDA (0.88 g, 2.79 mmol) was suspended in benzene (70 mL) at room temperature and $[(Me_3Si)_2N]BCl_2$ (0.67 g, 2.79 mmol) was added dropwise via syringe. After the reaction was stirred for 6 h all volatile components were removed in high vacuum and the residue was taken up in hexane (30 mL). After filtration 0.35 g (35%) **4a** was obtained at −30 °C as dark red crystals. **For 4a**: ^{1}H NMR (500 MHz, C_6D_6, 20 °C) δ 4.41, 3.91 (2 m, 8H, Cp), 0.37 (s, 18 H, $SiMe_3$); ^{13}C NMR (126 MHz, C_6D_6, 20 °C) δ 77.1, 72.4 (Cp), 45.0 (*ipso*-C), 5.1 ($SiMe_3$); ^{11}B NMR (160 MHz, C_6D_6, 20 °C) δ 48.3; UV/vis (hexanes) λ_{max} (ϵ) 479 nm (593 L $mol^{-1}cm^{-1}$); MS (70 eV) *m*/*z* (%) 355 (100) [M^+], 340 (80) [$M^+ - CH_3$], 299 (70) [$M^+ - Fe$], 73 (30) [$SiMe_3$]. For $C_{16}H_{26}BFeNSi_2$: calcd C 54.10, N 3.94, H 7.38; found C 53.43, N 4.13, H 7.79.

Reaction of Dilithioferrocene·*n*TMEDA with [*t*Bu$(Me_3Si)N]BCl_2$: $Fe(\eta^5\text{-}C_5H_4Li)_2$·TMEDA (1.01 g, 3.21 mmol) was suspended in benzene (70 mL) at room temperature. [*t*Bu$(Me_3Si)N]BCl_2$ (0.73 g, 3.21 mmol) was added dropwise via syringe. After the reaction was stirred for 6 h all volatile components were removed in high vacuum and the residue was taken up in hexane (30 mL). After filtration, 0.48 g (44%) of **4b** was obtained at −50 °C as dark red crystals.

For 4b: ^{1}H NMR (500 MHz, C_6D_6, 25 °C) δ 4.42, 4.40, 3.94, 3.92 (4 m, 8H, Cp), 1.50 (s, 9H, *t*Bu), 0.43 (s, 9H, $SiMe_3$); ^{13}C{^{1}H} NMR (75 MHz, C_6D_6, 25 °C) δ 76.7, 76.6, 72.8, 72.0 (Cp), 57.9 (CMe_3), 46.1, 44.3 (*ipso*-C), 34.6 (CMe_3), 7.5 ($SiMe_3$); ^{11}B{^{1}H} NMR (160 MHz, C_6D_6, 25 °C) δ 44.7; UV/vis (hexane) λ_{max} 489 nm (ϵ 765 L $mol^{-1}cm^{-1}$). For $C_{17}H_{26}BFeNSi$: calcd C 60.21; N 4.13, H 7.73; found C 58.70, N 4.00, H 7.89.

Reaction of Dilithioferrocene·*n*TMEDA with *i*Pr_2NBCl_2. A solution of *i*Pr_2NBCl_2 (3.7 g, 20.3 mmol) in hexanes (150 mL) was added dropwise to a suspension of $Fe(\eta^5\text{-}C_5H_4Li)_2$·TMEDA (6.4 g, 20.3 mmol) in hexanes (250 mL) at room temperature. After addition of the dichloroborane solution the reaction mixture was allowed to stir for another 15 min before being vacuum filtered through a fritted glass disk. 2.3 g (38%) of **4c** was obtained from the filtrate at −50 °C as dark red microcrystals.

For 4c: ^{1}H NMR (200 MHz, C_6D_6, 20 °C) δ 4.45, 4.06 (m, 8 H, Cp), 3.84 (sept., J(H,H) = 4.6 Hz, 2 H, N{C*H*$(CH_3)_2\}_2$), 1.20 (d, J(H,H) = 4.6 Hz, 12 H, N{CH(C*H*$_3)_2\}_2$); ^{13}C{^{1}H} NMR (75 MHz, C_6D_6, 20 °C) δ 77.0, 73.9 (Cp), 48.2 (N{*C*H$(CH_3)_2\}_2$), 44.2 (*ipso*-Cp), 24.3 (N{CH(*C*H$_3)_2\}_2$); ^{11}B{^{1}H} NMR (160 MHz, C_6D_6, 20 °C) δ 40.0; UV/vis (hexane) λ_{max} 498 nm (ϵ 775 L$mol^{-1}cm^{-1}$); MS (70 eV) *m*/*z* (%) 295 (100) [M^+], 252 (89) [$M^+ - i$Pr], 196 (53) [$MH^+ - Ni$Pr$_2$].

Attempted Reaction of 4b with $Pt(COD)_2$. $Pt(COD)_2$ (0.060 g, 0.15 mmol) and **4b** (0.050 g, 0.15 mmol) were combined in 1 mL of C_6D_6

(40) te Velde, G.; Baerends, E. J. *J. Comput. Phys.* **1992**, *99*, 84.
(41) Vosko, S. H.; Wilk, L.; Nusair, M. *Can. J. Phys.* **1990**, *58*, 1200.
(42) Becke, A. D. *Phys. Rev.* **1988**, *A38*, 3098.
(43) Perdew, J. P. *Phys. Rev.* **1986**, *B33*, 8822.
(44) Fan, L.; Ziegler, T. *J. Chem. Phys.* **1991**, *95*, 7401.
(45) Bishop, J. J.; Davison, A.; Katscher, M. L.; Lichtenberg, R. E.; Merill, J. C.; Smart, J. *J. Organomet. Chem.* **1971**, *27*, 241.
(46) Pietsch, E. H. E.; Kotowski, A.; Becke-Goering, M. *Gmelin Handbuch der Anorganischen Chemie*; Springer-Verlag: Berlin, Heidelberg, New York, 1979.
(47) Neilson, R. H.; Wells, R. L. *Synth. Inorg. Met. Org. Chem.* **1973**, *3*, 283.
(48) Geymayer, P.; Rochow, E. G.; Wannagat, U. *Angew. Chem.* **1964**, *76*, 499.
(49) Massey, J.; Power, K. N.; Manners, I.; Winnik, M. A. *J. Am. Chem. Soc.* **1998**, *120*, 9533.

Table 7. Crystal Data and Structure Refinement for **4a**, **4c**, **7**, and **8**

	4a	**4c**	**7**	**8**
formula	$C_{16}H_{26}BFeNSi_2$	$C_{16}H_{22}BFeN$	$C_{20}H_{22}BFe_2NO_4$	$C_{25}H_{26}BCo_2FeNO_8Si$
M_r	355.22	295.01	462.91	681.08
T, K	100	100.0(1)	203	100.0(1)
wavelength, Å	λ(Mo Kα) = 0.71069	λ(Mo Kα) = 0.71073	λ(Mo Kα) = 0.71073	λ(Mo Kα) = 0.71073
crystal system	monoclinic	triclinic	monoclinic	orthorhombic
space group	$P2_1/c$	$P\bar{1}$	$P2_1/n$	$Pbcn$
a, Å	11.614(1)	6.0733(3)	11.493(3)	29.3440(3)
b, Å	11.506(1)	13.5299(10)	12.565(5)	14.2428(2)
c, Å	13.601(1)	17.7040(13)	14.817(4)	13.8842(6)
α, deg	90	84.051(3)	90	90
β, deg	98.526(2)	87.394(4)	105.47(2)	90
γ, deg	90	82.095(4)	90	90
V, Å^3	1797	1432.45(17)	2062(1)	5802.8(3)
Z	4	4	4	8
ρ_{calc}, g cm^{-3}	1.31	1.368	1.49	1.559
μ(Mo Kα), mm^{-1}	0.962	1.037	1.43	1.711
F(000)	752	624	952	2768
crystal size, mm	0.21 × 0.26 × 0.31	0.15 × 0.14 × 0.12	0.40 × 0.31 × 0.05	0.30 × 0.30 × 0.20
diffractometer	Nonius DIP2020	Kappa CCD	Nonius CAD4	Kappa CCD
refinement on	F	F^2	F	F^2
θ range, deg	1−27	4.08−25.32	327	4.10−27.49
reflns collected	18806	17971	7482	40885
independent reflns	3605	5198	4000	6628
data/parameters	3189/235	5198/351	3034/253	6628/353
GOF	1.056	0.957	0.970	1.093
$R1$[a]	0.028 ($I > 3\sigma(I)$)	0.0511 ($I > 2\sigma(I)$)	0.051 ($I > \sigma(I)$)	0.0342 ($I > 2\sigma(I)$)
$wR2$[b]/R_w[c]	0.035[c]	0.1314[b]	0.048[c]	0.0821[b]
peak/hole (eÅ^{-3})	0.46/−0.46	0.814/−0.640	0.50	0.657/−0.480

[a] $R1 = \sum||F_o| - |F_c||/\sum|F_o|$. [b] $wR2 = \{\sum[w(F_o^2 - F_c^2)^2]/\sum[w(F_o^2)^2]\}^{1/2}$. [c] $R_w = \sum[w^{1/2}(|F_o| - |F_c|)]/\sum[w^{1/2}|F_o|]$.

in an NMR tube. NMR spectra taken after 0.5 and 1.0 h showed no reaction had taken place. After the solution was warmed to 40 °C for approximately 6 h, the ^{1}H NMR spectrum showed that decomposition of $Pt(COD)_2$ had occurred whereas **4c** remained unchanged.

Attempted Reaction of 4c with Karstedt's Catalyst. Approximately 1 mol % Karstedt's catalyst in xylenes was added to **4c** (0.020 g, 0.07 mmol) in an NMR tube containing approximately 1 mL of C_6D_6. NMR spectral data taken after 1 h and after an additional 24 h period showed only unreacted **4c**.

Reaction of 4c with MeOH. In a representative reaction MeOH (34 μL, 0.84 mmol) was added dropwise to a solution of **4c** (125 mg, 0.42 mmol) in hexanes (200 mL) at room temperature. The reaction mixture was stirred for 72 h. Periodic analysis by ^{1}H and ^{11}B NMR spectroscopy showed the formation of a complex mixture of products which could not be separated or structurally assigned. Modified reaction conditions (−78, 0 °C) and molar ratios (1 equiv or excess MeOH) resulted in the formation of similar mixtures of products.

Reaction of 4c with HCl. In a representative reaction, a solution of HCl in Et_2O (0.64 mL, 1.0 M, 0.64 mmol) was added dropwise to a solution of **4c** (200 mg, 0.68 mmol) in hexanes (50 mL) at −78 °C. The reaction mixture was stirred for 3 h. Analysis by ^{1}H and ^{11}B NMR spectroscopy showed the formation of a complex mixture of products which could not be separated or structurally assigned.

Reaction of 4c with $Fe(CO)_5$. A solution of $Fe(CO)_5$ (4.9 g, 25 mmol) in THF was added to **4c** (3.0 g, 10 mmol) in THF at −30 °C and irradiated with UV light. Upon warming to room temperature the reaction mixture turned dark red. The solvent was removed under high vacuum leaving a black solid, which was redissolved in toluene (60 mL). Deep red crystals of **7** (1.2 g, 26%) were isolated from this solution at −80 °C. Crystals for single-crystal X-ray diffraction studies were obtained by recrystallization from mesitylene at 0 °C.

For 7: ^{1}H NMR (500 MHz, $CDCl_3$, 20 °C) δ 5.36 (br.m, 4 H, Cp), 4.89 (br.m, 4 H, Cp), 3.49 (br.m, 2H, $-CH(CH_3)_2$), 1.05 (br.m, 12 H, $(CH(CH_3)_2)$); $^{13}C\{^1H\}$ NMR (126 MHz, $CDCl_3$, 20 °C) δ 239.2 (CO), 95.6 (Cp), 83.8 (Cp), 49.6 ($CH(CH_3)_2$), 23.8 ($CH(CH_3)_2$); $^{11}B\{^1H\}$ NMR (160 MHz, C_6D_6, 20 °C) δ 37.5; MS (70 eV) m/z (%) 463 (100) [M^+], 435 (9) [$M^+ - CO$], 407 (38) [$M^+ - 2CO$], 379 (28) [$M^+ - 3CO$], 351 (38) [$M^+ - 4CO$], 308 (100) [$M^+ - 4CO - i$Pr]; IR $\bar{\nu}$ 1990 (CO), 1781 (μ-CO). For $C_{20}H_{22}BFe_2NO_4$: calcd C 51.88, H 4.79, N 3.03; found C 51.58, H 4.71, N 2.90.

Reaction of 4c with $Fe_2(CO)_9$. Diironnonacarbonyl (0.135 g, 0.37 mmol) and **4c** (0.050 g, 0.17 mmol) were placed in 25 mL of THF. After the reaction was stirred for 16 h at room temperature a ^{1}H NMR spectrum (C_6D_6) showed peaks indicative of the formation of **7**. The red-black crystalline solid was isolated from 50:50 hexanes/toluene at −30 °C in 64% yield (0.050 g, 0.11 mmol).

Reaction of 4b with $Co_2(CO)_8$. Dicobaltoctacarbonyl (0.110 g, 0.32 mmol) and **4b** (0.100 g, 0.30 mmol) were dissolved in 3 mL of C_6D_6. After 1 h the ^{1}H NMR spectrum showed the formation of **8** in greater than 97% spectroscopic yield. The solvent was then removed, and the product taken up in hexanes. A small amount of insoluble material was removed via filtration of the resulting solution through glass wool and dark brown crystals of **8** were obtained at −30 °C (100 mg; 50% yield).

For 8: ^{1}H NMR (400 MHz, C_6D_6, 20 °C) δ 5.26 (br.s, 1 H, Cp), 5.21 (br.s, 1 H, Cp), 5.02 (br.s, 1 H, Cp), 4.96 (br.s, 1 H, Cp), 4.75 (br.s, 2 H, Cp), 4.53 (br.s, 1 H, Cp), 4.49 (br.s, 1 H, Cp), 1.16 (s, 9 H, *t*Bu), 0.12 (s, 9 H, $SiMe_3$); $^{13}C\{^1H\}$ NMR (75 MHz, C_6D_6, 20 °C) δ 211.8 (Fe-*C*O), 204.3, 201.3 (Co-*C*O), 92.9, 92.8, 91.6, 91.4, 90.3, 89.9, 89.9, 89.3 (Cp), 56.2 ($C(CH)_3$), 34.5 ($C(CH)_3$), 6.1 ($SiMe_3$), not observed (*ipso*-Cp); $^{11}B\{^1H\}$ NMR (160 MHz, C_6D_6, 20 °C) δ 49.6; ^{29}Si NMR (79.3 MHz, C_6D_6, 20 °C) δ 0.0; IR (hexanes, 25 °C) $\bar{\nu}$ (cm^{-1}) 2070, 2064, 2055, 2031, 2016, 1979 (CO); 1896, 1867, 1830, 1779 (μ-CO).

Thermal Polymerization of 4a and 4b. Similar results were obtained for both **4a** and **4b** except in the latter case only insoluble material was formed. Only the procedure for **4a** is given.

An 80 mg (0.23 mmol) sample of monomer **4a** was heated to 180 °C in a sealed, evacuated Pyrex tube. After about 15 min the contents of the tube melted and subsequently became increasingly viscous, becoming immobile after 2 h. The resulting red glassy material **9a** was found to be essentially insoluble in common organic solvents. A small amount of **9a** was extracted into C_6D_6.

Pyrolysis MS of the crude product (70 eV, 450 °C): m/z (%) 1065 (45) [$n = 3$], 710 (100) [$n = 2$], 355 (78) [$n = 1$], 73 (80) [$SiMe_3$].

For 9a: soluble fraction, ^{1}H NMR (400 MHz, C_6D_6, 20 °C) δ 4.19, 4.26, 4.38, 4.53, 4.66, 4.94 (6 ps.t, Cp), 0.25, 0.33, 0.46 (3 s, $SiMe_3$); insoluble fraction, solid state $^{13}C\{^1H\}$ NMR (100.6 MHz, 20 °C) δ 77.6, 74.1 (Cp), 5.1 ($SiMe_3$), not observed (*ipso*-Cp).

Thermal Polymerization of 4c. A 500 mg (1.69 mmol) sample of monomer **4c** was heated to 200 °C in a sealed, evacuated Pyrex tube. After ca. 30 min the contents of the tube had melted and subsequently became increasingly viscous. After 1 h the contents of the tube were found to be completely immobile. The dark red, glassy product was found to be soluble in polar organic solvents such as toluene, THF, CH_2Cl_2, and $CHCl_3$. ^{1}H NMR spectroscopy revealed the formation of three products, which were assigned as polymer **9c**, a cyclic dimer, and a cyclic trimer by comparison with an independently prepared sample of the dimer[38] and by mass spectrometry. Precipitation into dry hexanes from toluene (twice) afforded pure polymer **9c**: yield 170 mg, 34%; spectroscopic yield ca. 50%.

MS of the crude product: (70 eV, 390 °C) *m*/*z* (%) 590 (100) [n = 2 (M_2)], 295 (7) [M_2^{2+}], 86 (84) [iPr$_2$]; (70 eV, 440 °C) *m*/*z* (%) 885 (8) [n = 3 (M_3)], 590 (100) [n = 2 (M_2)], 295 (7) [M_2^{2+}], 86 (17) [iPr$_2$].

For cyclic dimer: ^{1}H NMR (400 MHz, C_6D_6, 20 °C) δ 4.68, 4.33 (br.s, 2 × 8 H, Cp), 3.78 (m, 4 H, CH), 1.03 (d, J(H,H) = 9.2 Hz, 24 H, CH_3)

For 9c: ^{1}H NMR (400 MHz, C_6D_6, 20 °C) δ 5.42 (br.m, 2 H, NC*H*$(CH_3)_2$), 4.29, 4.25 (2 s, 8 H, Cp), 1.41 (d, J(H,H) = 4.6 Hz, 12 H, NCH(C*H*$_3)_2$); ^{13}C{^{1}H} NMR (126 MHz, C_6D_6, 20 °C) δ 77.5 (Cp), 71.1 (Cp), 50.6 (*C*H$(CH_3)_2$), 26.5 (CH(*C*H$_3)_2$); ^{11}B{^{1}H} NMR (160 MHz, C_6D_6, 20 °C) δ 41.5. A cross-peak was observed in the HSQC spectrum between the tertiary ^{i}Pr group carbon atom (50.6 ppm) and the proton resonance at 5.42 ppm confirming the connectivity of these atoms. A cross-peak was also observed in the COSY spectrum between the proton on the tertiary ^{i}Pr carbon (5.42 ppm) and the protons of the CH_3 substituents (1.41 ppm).

Crystal Structure Determinations for 4a, 4c, 7, and 8: Crystal data and details of the measurements are summarized in Table 7. The structures were solved by direct methods (SHELXS97) and refined by full-matrix least squares (SHELXL97) based on F2 with all reflections. Non-hydrogen atoms were refined anisotropically, and hydrogen atoms were included in calculated positions.

Crystallographic data (excluding structure factors) for the structures reported in this paper have been deposited with the Cambridge Crystallographic Data Centre as supplementary publication no. CCDC-100378 (**4a**), 144426 (**4c**), 134373 (**7**), and 134374 (**8**). Copies of the data can be obtained free of charge on application to CCDC, 12 Union Road, Cambridge CB2 1EZ, UK (fax: (+44) 1223 336−033; e-mail: deposit@ccdc.cam.ac.uk).

Acknowledgment. This paper is dedicated to Prof. Peter Paetzold on the occasion of his 65th birthday. We wish to acknowledge a DFG postdoctoral fellowship for F.J. and a University of Toronto Open Fellowship for A.B. I.M. is grateful to NSERC for an E. W. R. Steacie Fellowship (1997−1999), the University of Toronto for a McLean Fellowship (1997−2003), and the Ontario Government for a PREA Award (1999−2003). H.B. thanks the Deutsche Forschungsgemeinschaft (DFG) and the Fonds der Chemischen Industrie for financial support. Part of this work has been carried out using computational resources of a DEC 8400 multiprocessor cluster (Columbus/Magellan), provided by the U.K. Computational Chemistry Facility at Rutherford Appleton Laboratory (administered by the Department of Chemistry, King's College London, Strand, London WC2R 2LS). The authors wish to thank Karen Temple for supplying the $Pt(COD)_2$ used in the reactivity studies, Dr. Tim Burrow for the 2D NMR studies, Dr. Hiltrud Grondey for the solid state NMR work, and Jason Massey for the dynamic light scattering analysis.

Supporting Information Available: Crystallographic data for compounds **4c**, **7**, and **8**, including tables of crystal data, atomic coordinates, bond lengths and angles, and anisotropic thermal parameters (PDF). This material is available free of charge via the Internet at http://pubs.acs.org.

JA000311+